Hindawi Publishing Corporation
Advances in High Energy Physics
Volume 2014, Article ID 725739, 14 pages
http://dx.doi.org/10.1155/2014/725739

Research Article

Transverse Momentum and Pseudorapidity Distributions of Charged Particles and Spatial Shapes of Interacting Events in Pb-Pb Collisions at 2.76 TeV

Fu-Hu Liu, Ya-Qin Gao, Tian Tian, and Bao-Chun Li

Institute of Theoretical Physics, Shanxi University, Taiyuan, Shanxi 030006, China

Correspondence should be addressed to Fu-Hu Liu; fuhuliu@163.com

Received 7 February 2014; Accepted 3 June 2014; Published 7 July 2014

Academic Editor: Bhartendu K. Singh

The transverse momentum and pseudorapidity distributions of charged particles produced in Pb-Pb collisions with different centrality intervals at center-of-mass energy per nucleon pair $\sqrt{s_{NN}} = 2.76$ TeV have been analyzed by using the improved multisource thermal model in which the whole interacting system and then the sources are described by the Tsallis statistics. The modelling results are in agreement with experimental data of the ALICE Collaboration. The rapidity distributions of charged particles are obtained according to the extracted parameter values. The shapes of interacting events (the dispersion plots of charged particles) are given in the momentum, rapidity, velocity, and coordinate spaces. Meanwhile, the event shapes in different spaces consisted by different transverse quantities and longitudinal quantities are presented.

1. Introduction

Because the Relativistic Heavy Ion Collider (RHIC) run successfully in 2000, the studies of high energy heavy ion collisions have been arriving in the collider era since then. Many experiments on heavy ion collisions in GeV energy region have been finished in the past years [1–4]. The center-of-mass energy per nucleon pair ($\sqrt{s_{NN}}$) at the RHIC is superlatively 200 GeV. Presently, the most powerful heavy-ion collider in the world, the Large Hadron Collider (LHC), was built successfully in 2008-2009. Recently, the LHC does perform successful experiments on proton-proton collision at total energy of 7 TeV, proton-lead collisions at $\sqrt{s_{NN}} = 5.02$ TeV, and lead-lead (Pb-Pb) collisions at $\sqrt{s_{NN}} = 2.76$ TeV [5–8].

Many experiments do measure distributions and correlations of multiplicities, pseudorapidities (rapidities), transverse momentums, azimuths, and others due to that they are the "first day" measurement quantities on charged particles. Generally, these "first day" measurement quantities are studied in different centrality intervals (impacting parameters), sizes of interacting systems, center-of-mass energies, and other available dependent quantities. These charged particles are divided into positively charged particles, negatively charged particles, charged mesons, charged baryons, protons, antiprotons, and other identified charged particles according to different classifications. Even if for the transverse momentum and pseudorapidity (rapidity) distributions of charged particles, we have different interacting mechanisms and distribution regions which are considered in modelling analyses.

The transverse momentum and pseudorapidity (rapidity) distributions of charged particles contain abundant information. Studies of transverse momentum and pseudorapidity (rapidity) distributions have been persisting from fixed target experiments at accelerators to collider experiments at the RHIC and LHC. Recently, the ALICE Collaboration reported the centrality dependences of the transverse momentum and pseudorapidity distributions for charged particles in Pb-Pb collisions at $\sqrt{s_{NN}} = 2.76$ TeV [8, 9]. We are interested in analyzing the ALICE data by using the current models

(for a collection of many models, see [10]), particularly the multisource thermal model which was proposed by us some years ago [11–13].

In this paper, we analyze the ALICE data on transverse momentum and pseudorapidity distributions of charged particles produced in Pb-Pb collisions at $\sqrt{s_{NN}} = 2.76$ TeV [8, 9] by using the improved multisource thermal model [11–13] in which the Boltzmann distribution is replaced by the Tsallis statistics [14–21]. The rapidity distributions of charged particles are obtained according to the extracted parameter values. The dispersion plots of charged particles, that is, the shapes of interacting events, are given in different spaces.

2. The Model and Method

In a given reference frame and in the rapidity space, in the framework of the multisource thermal model [11–13], many emission sources with different rapidities y_x are assumed to form in high energy collisions. According to the values of y_x, a target cylinder in rapidity interval $[y_{T\min}, y_{T\max}]$, a projectile cylinder in rapidity interval $[y_{P\min}, y_{P\max}]$, a leading target nucleon cylinder in rapidity interval $[y_{LT\min}, y_{LT\max}]$, and a leading projectile nucleon cylinder in rapidity interval $[y_{LP\min}, y_{LP\max}]$ are assumed to form. For a symmetric collision system, we have equal relations $y_{T\min} = -y_{P\max}$, $y_{T\max} = -y_{P\min}$, $y_{LT\min} = -y_{LP\max}$, and $y_{LT\max} = y_{LP\min}$.

In the original multisource thermal model [11–13], we have used in fact a multitemperature relativistic ideal gas model which expects a few local thermal equilibrium states existing in the collisions. Each local equilibrium state can be described by the relativistic ideal gas model (Boltzmann distribution) [22, 23] with a given temperature, and the emission of particles in the rest frame of the considered source is isotropic. This multitemperature picture can be described by the Tsallis statistics [14–21] which describes the invariant particle momentum (p') distribution in the rest frame of the considered source to be

$$E'\frac{d^3N}{d^3p'} = C_1\sqrt{p'^2+m_0^2} \times \left[1+(q-1)\frac{\sqrt{p'^2+m_0^2}-\mu}{T}\right]^{-q/(q-1)}, \quad (1)$$

where C_1 is the normalization constant of the distribution, N is the particle number, T is the temperature parameter of the source, q is a parameter (an entropic index) to characterize the degree of nonequilibrium, and E', m_0, and μ are, respectively, the energy, rest mass, and chemical potential of the considered particle. At LHC energies, the chemical potential can be neglected due to its small value. The real free parameters in (1) are then T and q. Because of the introduction of the Tsallis statistics, the multisource thermal model is improved by us.

We can use the Monte Carlo method to perform the calculation based on the probability distribution $f(p')$ of momentums

$$f(p') = \frac{1}{N}\frac{dN}{dp'} = C_2 p'^2 \times \left[1+(q-1)\frac{\sqrt{p'^2+m_0^2}-\mu}{T}\right]^{-q/(q-1)}, \quad (2)$$

where C_2 is the normalization constant. Because (2) is the probability distribution of momentums and (1) is the invariant momentum distribution, they are different in the prefactors. In the calculation, in the rest frame of the considered source with rapidity shift y_x, various quantities such as azimuth ϕ', space angle θ', momentum p', longitudinal momentum p'_z, and energy E' can be obtained. In the laboratory or center-of-mass reference frame, the rapidity $y = y_x + (1/2)\ln[(E'+p'_z)/(E'-p'_z)]$, the transverse momentum $p_T = p'\sin\theta'$, the x-component of momentum $p_x = p_T\cos\phi'$, the y-component of momentum $p_y = p_T\sin\phi'$, the longitudinal momentum $p_z = \sqrt{p_T^2+m_0^2}\sinh y$, the energy $E = \sqrt{p_T^2+m_0^2}\cosh y$, the space angle $\theta = \arctan(p_T/p_z)$, and the pseudorapidity $\eta = -\ln\tan(\theta/2)$ can be obtained. Meanwhile, the velocity components $\beta_x = p_x/E$, $\beta_y = p_y/E$, and $\beta_z = p_z/E$, as well as the coordinate components $x = t_0\beta_x$, $y = t_0\beta_y$, and $z = t_0\beta_z$ can be obtained, where t_0 denotes the time interval from initial collision to the stage of freeze-out. To extract more information in the calculation, we define the rapidity in x-direction $y_1 = (1/2)\ln[(E+p_x)/(E-p_x)]$, the rapidity in y-direction $y_2 = (1/2)\ln[(E+p_y)/(E-p_y)]$, the transverse rapidity $y_T = (1/2)\ln[(E+p_T)/(E-p_T)]$, the transverse velocity $\beta_T = p_T/E$, and the transverse coordinate $r_T = t_0\beta_T$.

In the following section, except for the descriptions of transverse momentum and pseudorapidity distributions and the extraction of rapidity distributions, we shall present the event shapes in momentum space $p_x(p_y) - p_z$, rapidity space $y_1(y_2) - y$, and velocity space $\beta_x(\beta_y) - \beta_z$ (rescaled coordinate space $x(y)/t_0 - z/t_0$). Meanwhile, the event shapes in some transverse quantities [p_T, y_T, β_T (r_T/t_0)] and longitudinal quantities [p_z, y, β_z (z/t_0)] spaces are presented, too. We would like to point out that we can obtain separately rapidity and pseudorapidity distributions in the calculation. We do not need to do a conversion between the two distributions. Except for nucleus-nucleus collisions, the Tsallis statistics is also used to deal with proton-proton collision in literature [24–26].

3. Comparison and Extraction

The transverse momentum distributions of $\pi^+ + \pi^-$, $K^+ + K^-$, and $p + \overline{p}$ produced in Pb-Pb collisions at $\sqrt{s_{NN}} = 2.76$ TeV in different centrality intervals are shown in Figures 1(a)–1(c), respectively, where N_{EV} denotes the number of events. From up data to low one in each panel, the corresponding centrality

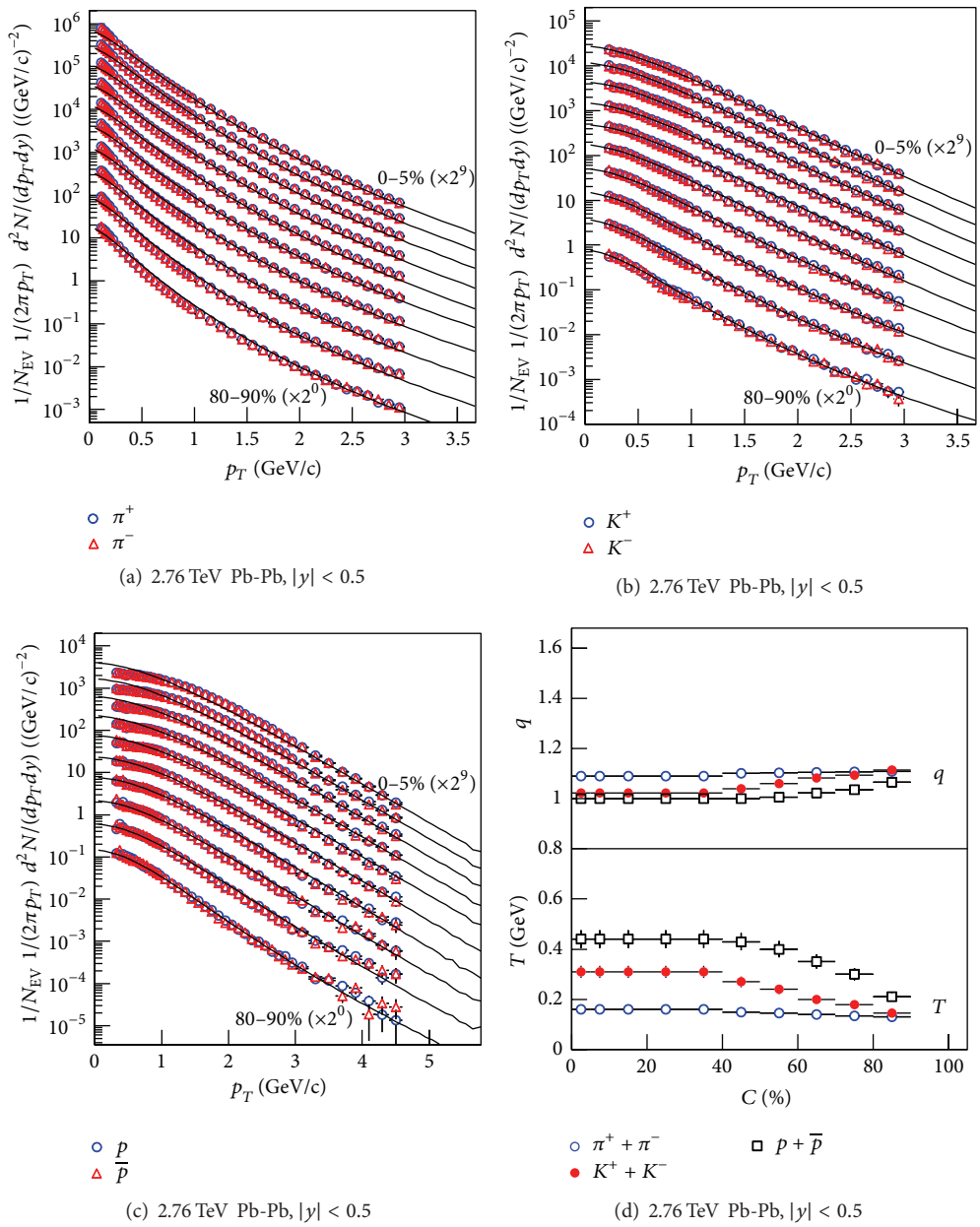

FIGURE 1: (a)–(c) Transverse momentum distributions of (a) $\pi^+ + \pi^-$, (b) $K^+ + K^-$, and (c) $p + \overline{p}$ produced in Pb-Pb collisions at $\sqrt{s_{NN}}$ = 2.76 TeV in different centrality intervals 0–5%, 5–10%, 10–20%, . . ., and 80–90% scaled by multiplying 2^9, 2^8, 2^7, . . ., and 2^0, respectively. The symbols represent the experimental data of the ALICE Collaboration [8] and the curves are results of the Tsallis statistics. (d) Dependences of parameters T and q on centrality intervals. Different symbols represent the parameter values extracted from the distributions of different charged particles.

intervals are 0–5%, 5–10%, 10–20%, . . ., and 80–90% scaled by multiplying 2^9, 2^8, 2^7, . . ., and 2^0, respectively. The symbols represent the experimental data of the ALICE Collaboration [8] measured in the rapidity region $|y| < 0.5$ and the curves are results of the Tsallis statistics. The fitted parameter values are listed in Table 1 with the values of χ^2/dof (per degree of freedom). To see clearly the dependences of parameters on centrality, the parameter values in Table 1 are also given in Figure 1(d). We can see that the temperature and nonequilibrium degree do not change in the centrality interval 0–40%. The temperature decreases and the nonequilibrium degree increases with increase of the centrality percentage in the interval 40–90%.

Figure 2 presents the pseudorapidity distributions of charged particles produced in Pb-Pb collisions at $\sqrt{s_{NN}}$ = 2.76 TeV, where N_{ch} denotes the number of charged particles.

Table 1: Values of parameters and χ^2/dof corresponding to the curves for $\pi^+ + \pi^-$, $K^+ + K^-$, and $p + \overline{p}$ in Figures 1(a)–1(c), respectively.

Centrality	Figure 1(a)			Figure 1(b)			Figure 1(c)		
	$T_{\pi^\pm}$ (GeV)	$q_{\pi^\pm}$	χ^2/dof	$T_{K^\pm}$ (GeV)	$q_{K^\pm}$	χ^2/dof	$T_{p(\overline{p})}$ (GeV)	$q_{p(\overline{p})}$	χ^2/dof
0–5%	0.16 ± 0.02	1.090 ± 0.020	0.489	0.31 ± 0.03	1.023 ± 0.015	0.402	0.44 ± 0.04	1.001 ± 0.001	2.140
5–10%	0.16 ± 0.02	1.090 ± 0.020	0.549	0.31 ± 0.03	1.023 ± 0.015	0.365	0.44 ± 0.04	1.001 ± 0.001	1.961
10–20%	0.16 ± 0.02	1.090 ± 0.020	0.633	0.31 ± 0.03	1.023 ± 0.015	0.377	0.44 ± 0.04	1.001 ± 0.001	1.568
20–30%	0.16 ± 0.02	1.090 ± 0.020	0.741	0.31 ± 0.03	1.023 ± 0.015	0.637	0.44 ± 0.04	1.001 ± 0.001	0.943
30–40%	0.16 ± 0.02	1.090 ± 0.020	0.885	0.31 ± 0.03	1.023 ± 0.015	1.539	0.44 ± 0.04	1.001 ± 0.001	0.682
40–50%	0.15 ± 0.02	1.100 ± 0.020	0.886	0.27 ± 0.03	1.040 ± 0.018	1.110	0.43 ± 0.04	1.001 ± 0.001	0.450
50–60%	0.15 ± 0.02	1.102 ± 0.020	1.157	0.24 ± 0.02	1.060 ± 0.018	0.880	0.40 ± 0.04	1.006 ± 0.005	0.613
60–70%	0.14 ± 0.01	1.104 ± 0.020	1.555	0.20 ± 0.02	1.082 ± 0.018	0.775	0.35 ± 0.04	1.022 ± 0.015	0.593
70–80%	0.14 ± 0.01	1.106 ± 0.020	1.874	0.18 ± 0.02	1.093 ± 0.020	0.879	0.30 ± 0.03	1.035 ± 0.018	0.609
80–90%	0.13 ± 0.01	1.108 ± 0.020	2.095	0.15 ± 0.02	1.114 ± 0.020	0.630	0.21 ± 0.02	1.065 ± 0.018	0.195

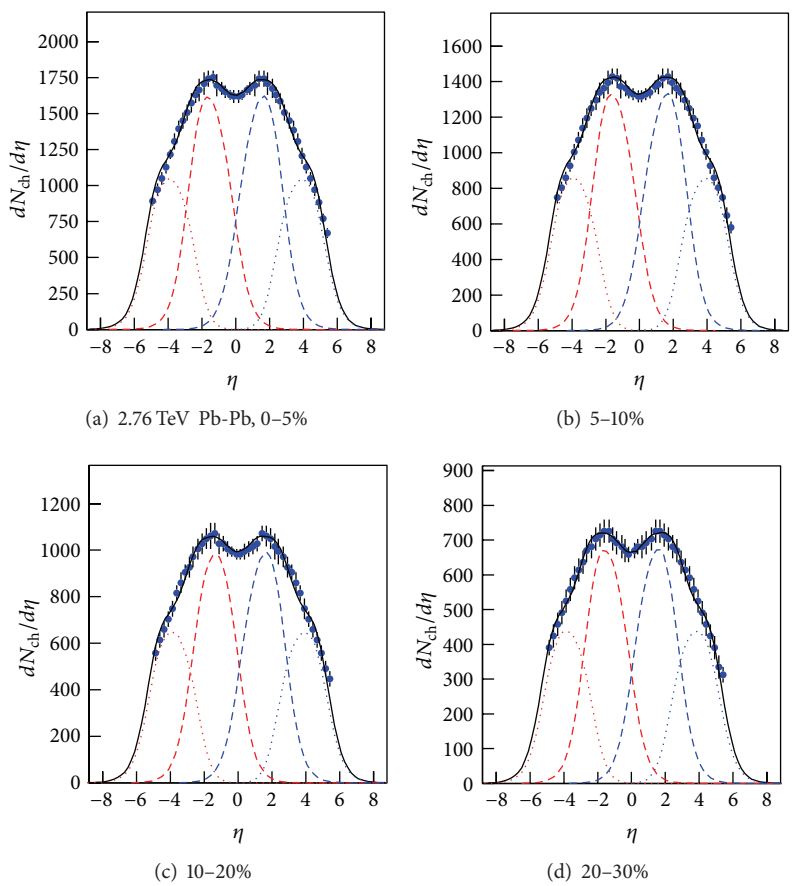

(a) 2.76 TeV Pb-Pb, 0–5%

(b) 5–10%

(c) 10–20%

(d) 20–30%

Figure 2: Pseudorapidity distributions of charged particles produced in Pb-Pb collisions at $\sqrt{s_{NN}}$ = 2.76 TeV in the centrality intervals (a) 0–5%, (b) 5–10%, (c) 10–20%, and (d) 20–30%. The circles represent the experimental data of the ALICE Collaboration [9], and the curves are our modelling results.

Figures 2(a)–2(d) correspond to the centrality intervals 0–5%, 5–10%, 10–20%, and 20–30%, respectively. The circles represent the experimental data of the ALICE Collaboration [9], and the curves are our results calculated by using the improved multisource thermal model in which the Tsallis statistics is adopted. From left to right in each panel, the dotted or dashed curves are orderly the contributions of leading target nucleons, target cylinder, projectile cylinder, and leading projectile nucleons, respectively; and the solid curve in each panel is the sum of the dotted and dashed

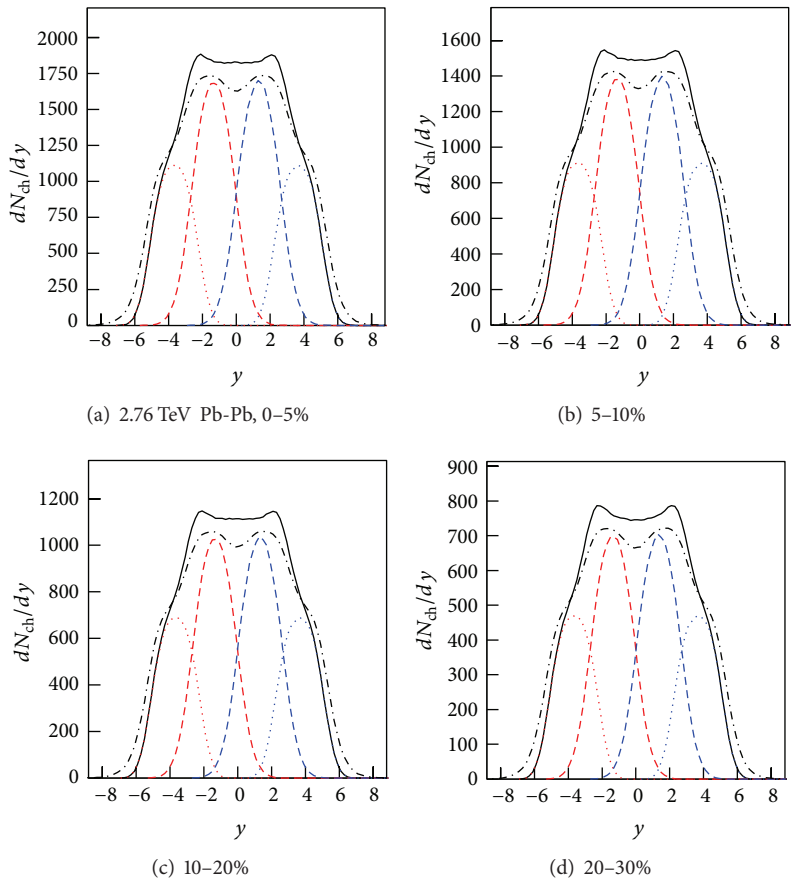

Figure 3: Extracted rapidity distributions of charged particles produced in Pb-Pb collisions at $\sqrt{s_{NN}} = 2.76$ TeV in the centrality intervals (a) 0–5%, (b) 5–10%, (c) 10–20%, and (d) 20–30%. The curves are our modelling results. Particularly, the dotted-dashed curves are pseudorapidity distributions taken directly from Figure 2.

curves. For the four panels, the parameter values obtained by fitting the experimental data are $y_{P\max} = 2.66 \pm 0.03$, $y_{P\min} = 0.03 \pm 0.01$, $y_{LP\max} = 5.10 \pm 0.03$, $y_{LP\min} = 2.25 \pm 0.02$, and $k = 0.199 \pm 0.002$. The other parameters $T_C = (0.16 \pm 0.02)$ GeV, $q_C = 1.090 \pm 0.003$, $T_L = (0.44 \pm 0.04)$ GeV, and $q_L = 1.001 \pm 0.001$ are approximately taken from Figure 1 (Table 1), where the indexes C and L denote the target/projectile cylinders and the leading target/projectile nucleon cylinders, respectively. The values of χ^2/dof are 0.120, 0.141, 0.110, and 0.109, respectively.

In the calculation for Figure 2, only the contributions of $\pi^+ + \pi^-$ for the target/projectile cylinders and those of $p + \overline{p}$ for the leading target/projectile nucleon cylinders are considered due to the other contributions being small. We take m_0 as the rest mass of a charged pion (or a proton) for the target/projectile cylinders (or the leading target/projectile nucleon cylinders). Another approximation is that the parameter values obtained in $|y| < 0.5$ (Figure 1) are used for a wide pseudorapidity range (Figure 2). The treatment for the target/projectile cylinders underestimates T_C by ~0.01 GeV and overestimates q_C by ~0.02. Contrarily, the second approximation overestimates T_L and underestimates q_L. In fact, the pseudorapidity distribution is not mainly determined by the temperature and degree of nonequilibrium but by the rapidity shifts and contribution ratio of leading nucleons. One can see that the model describes the pseudorapidity distributions of charged particles produced in Pb-Pb collisions at the LHC energy. The rapidity shifts, contribution ratio of leading nucleons, temperature, and degree of nonequilibrium do not depend obviously on the centrality percentage in the considered centrality interval 0–30%.

According to the parameter values extracted from the pseudorapidity distributions, we present the rapidity distributions of charged particles in Figure 3. For the purpose of comparison, the pseudorapidity distributions presented in Figure 2 are directly presented in Figure 3 by the dotted-dashed cures. The meanings of other curves in Figure 3 are the same as those in Figure 2. One can see the difference between the rapidity and pseudorapidity distributions of

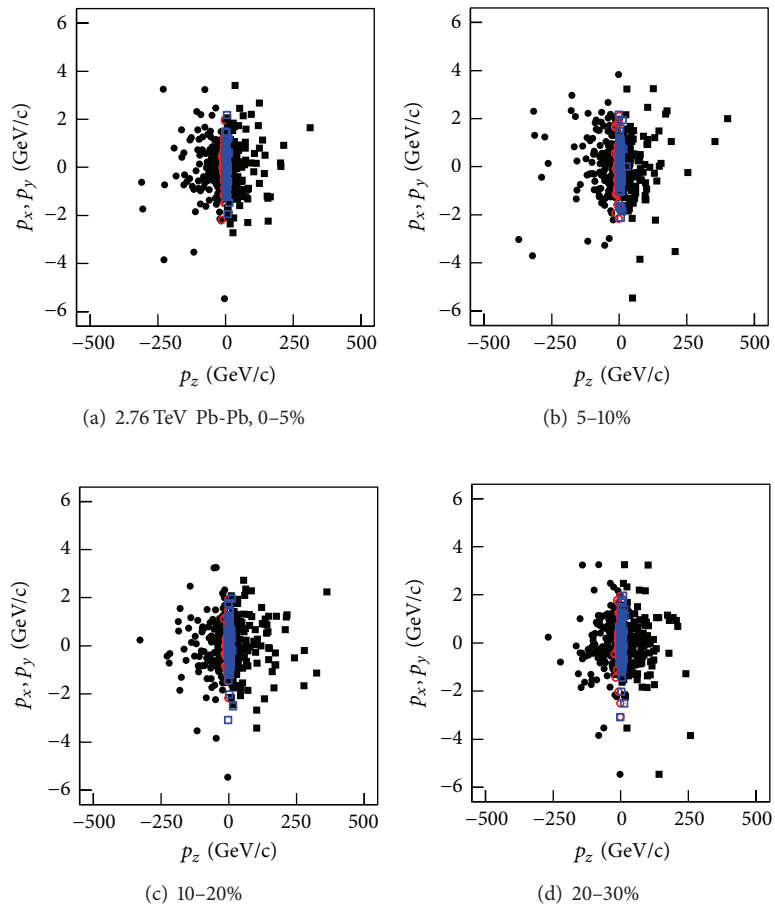

Figure 4: Extracted event shapes (dispersion plots) of 1000 charged particles at the stage of freeze-out in the momentum space $p_x - p_z$ (or $p_y - p_z$) in Pb-Pb collisions at $\sqrt{s_{NN}} = 2.76$ TeV in the centrality intervals (a) 0–5%, (b) 5–10%, (c) 10–20%, and (d) 20–30%. The closed circles, open circles, open squares, and closed squares represent orderly the contributions of leading target nucleons, target cylinder, projectile cylinder, and leading projectile nucleons from low to high in the longitudinal rapidity space.

charged particles produced in Pb-Pb collisions at $\sqrt{s_{NN}} = 2.76$ TeV. The differences among the four centrality intervals are not obvious except for the normalization.

The event shapes (dispersion plots) obtained from 1000 charged particles at the stage of freeze-out in the momentum space $p_x - p_z$ (or $p_y - p_z$), rapidity space $y_1 - y$ (or $y_2 - y$), and velocity space $\beta_x - \beta_z$ (or $\beta_y - \beta_z$) in Pb-Pb collisions in different centrality intervals at $\sqrt{s_{NN}} = 2.76$ TeV are displayed in Figures 4(a)–4(d), 5(a)–5(d) and 6(a)–6(d), respectively. If we rescale coordinates x, y, and z to x/t_0, y/t_0, and z/t_0, respectively, Figure 6 is also the event shapes in (rescaled) coordinate space $x/t_0 - z/t_0$ (or $y/t_0 - z/t_0$). In the three figures, the closed circles, open circles, open squares, and closed squares correspond to the contributions of leading target nucleons, target cylinder, projectile cylinder, and leading projectile nucleons, respectively. One can see that the densities in the small momentum components, small y_1 (y_2) and large y, small β_x (β_y) and large β_z, and small x (y) and large z regions are larger than those in other regions. The event shapes (dispersion plots) in the momentum, rapidity, and velocity (coordinate) spaces are obviously different. The differences in event shapes (relative density distributions in the dispersion plots) for different centrality intervals are not obvious for the considered collisions.

To extract more information from the pseudorapidity distributions, we present the event shapes (dispersion plots) from 1000 charged particles in Pb-Pb collisions in different centrality intervals at $\sqrt{s_{NN}} = 2.76$ TeV in some spaces consisted by different transverse quantities and different longitudinal quantities. Figures 7, 8, and 9 present the results in $p_T - p_z$, $y_T - p_z$, and $\beta_T - p_z$ ($r_T/t_0 - p_z$) spaces, respectively, Figures 10, 11, and 12 present the results in $p_T - y$, $y_T - y$, and $\beta_T - y$ ($r_T/t_0 - y$) spaces, respectively, and Figures 13, 14, and 15 present the results in $p_T - \beta_z$ ($p_T - z/t_0$), $y_T - \beta_z$ ($y_T - z/t_0$), and $\beta_T - \beta_z$ ($\beta_T - z/t_0$ or $r_T/t_0 - \beta_z$ or $r_T/t_0 - z/t_0$) spaces, respectively. The meanings of the symbols in Figures 7–15 are the same as those in Figure 4. We see different events shapes (relative density distributions in the dispersion plots)

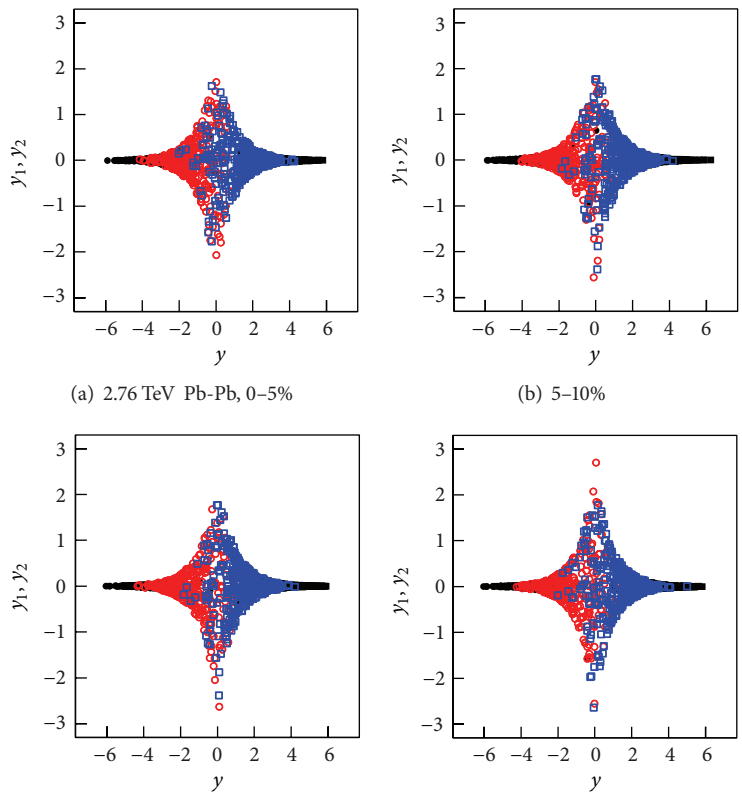

(a) 2.76 TeV Pb-Pb, 0–5%

(b) 5–10%

(c) 10–20%

(d) 20–30%

Figure 5: The same as for Figure 4, but showing the results in the rapidity space $y_1 - y$ (or $y_2 - y$).

in different spaces consisted by different transverse quantities and different longitudinal quantities. The results in the same space for different centrality intervals are not obvious due to almost the same extracted parameters (except the total particle number).

Although we have not compared more predicted results with experimental data in the present work, the improved multisource thermal model which adopts the Tsallis statistics can describe both the transverse momentum distribution and the pseudorapidity (rapidity) distribution in high energy collisions. The transverse momentum distribution is mainly determined by the temperature and nonequilibrium degree, and the pseudorapidity distribution is mainly determined by the rapidity shifts and contribution ratio of leading nucleons.

There are some fluctuations in our calculation by using the Monte Carlo method. For example, for an event with a given centrality, different sets of random numbers render different dispersion plots, which are small statistical fluctuations from event to event. The events with different centralities correspond to large statistical fluctuations from event to event. In some case, different events may have different interacting mechanisms, which render dynamical fluctuations from event to event. The present work concerns only the statistical fluctuations.

4. Conclusions

From the above discussions, we obtain following conclusions.

(a) The transverse momentum distributions of charged particles produced in Pb-Pb collisions with centrality intervals from 0–5% to 80–90% at $\sqrt{s_{NN}} = 2.76$ TeV have been analyzed by using the improved multisource thermal model in which the whole interacting system and then the sources are described by the Tsallis statistics [14–21]. The modelling results are in agreement with the experimental data of the ALICE Collaboration [8]. In the centrality intervals from 0–5% to 30–40%, the temperature and nonequilibrium degree do not show a change. In the centrality intervals from 40–50% to 80–90%, the temperature decreases and the nonequilibrium degree increases with increase of the centrality percentage.

(b) The pseudorapidity distributions of charged particles produced in Pb-Pb collisions with centrality intervals from 0–5% to 20–30% at $\sqrt{s_{NN}} = 2.76$ TeV have been analyzed by using the improved multisource thermal model, too. The modelling results are in agreement with the experimental data of the ALICE

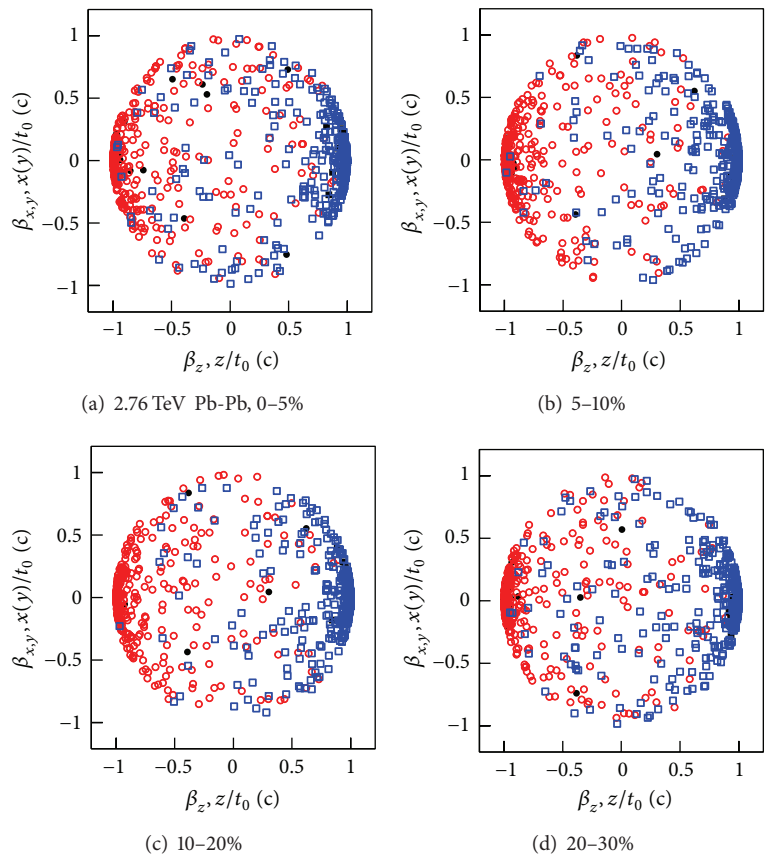

FIGURE 6: The same as for Figure 4, but showing the results in the velocity space $\beta_x - \beta_z$ (or $\beta_y - \beta_z$) or the rescaled coordinate space $x/t_0 - z/t_0$ (or $y/t_0 - z/t_0$).

Collaboration [9]. The contributions of the leading target nucleons, target cylinder, projectile cylinder, and leading projectile nucleons are given in different regions in the rapidity space. The rapidity shifts and contribution ratio of leading nucleons do not depend obviously on the centrality percentage in the intervals from 0–5% to 20–30%.

(c) Based on the parameter values extracted from the transverse momentum and pseudorapidity distributions, the rapidity distributions of charged particles produced in Pb-Pb collisions with different centrality intervals at $\sqrt{s_{NN}} = 2.76$ TeV are obtained. The contributions of the leading target nucleons, target cylinder, projectile cylinder, and leading projectile nucleons are given in different regions in the rapidity space. The rapidity shifts and contribution ratio of leading nucleons do not depend obviously on the centrality percentage in the intervals from 0–5% to 20–30%.

(d) The event shapes (dispersion plots) at the stage of freeze-out in the momentum space $p_x - p_z$ (or $p_y - p_z$), rapidity space $y_1 - y$ (or $y_2 - y$), velocity space $\beta_x - \beta_z$ (or $\beta_y - \beta_z$), and coordinate space $x/t_0 - z/t_0$ (or $y/t_0 - z/t_0$) in Pb-Pb collisions in different centrality intervals at $\sqrt{s_{NN}} = 2.76$ TeV are presented. The densities in the small momentum components, small y_1 (y_2) and large y, small β_x (β_y) and large β_z, and small x (y) and large z regions are larger than those in other regions. The event shapes (dispersion plots) in the momentum, rapidity, velocity (coordinate) spaces are obviously different. The differences in event shapes (density distributions in the dispersion plots) for different centrality intervals are not obvious for the considered collisions in the considered intervals from 0–5% to 20–30%.

(e) The event shapes (dispersion plots) in Pb-Pb collisions in different centrality intervals at $\sqrt{s_{NN}} = 2.76$ TeV in other spaces including $p_T - p_z$, $y_T - p_z$, $\beta_T - p_z$ ($r_T/t_0 - p_z$), $p_T - y$, $y_T - y$, $\beta_T - y$ ($r_T/t_0 - y$), $p_T - \beta_z$ ($p_T - z/t_0$), $y_T - \beta_z$ ($y_T - z/t_0$), and $\beta_T - \beta_z$ ($\beta_T - z/t_0$ or $r_T/t_0 - \beta_z$ or $r_T/t_0 - z/t_0$) spaces are presented. Different events shapes (density distributions in the dispersion plots) in different spaces consisted by different transverse quantities and different longitudinal quantities are

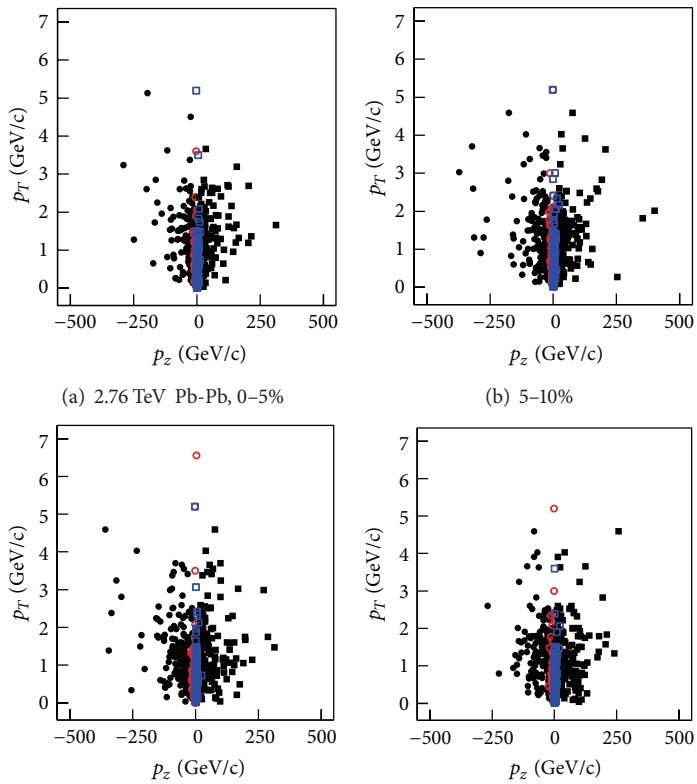

(a) 2.76 TeV Pb-Pb, 0–5%

(b) 5–10%

(c) 10–20%

(d) 20–30%

FIGURE 7: The same as for Figure 4, but showing the results in the space $p_T - p_z$.

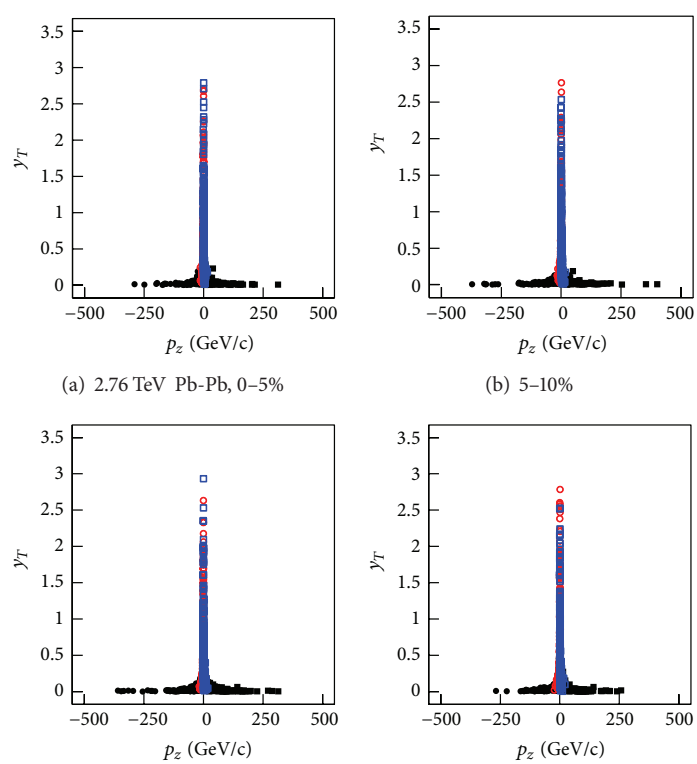

(a) 2.76 TeV Pb-Pb, 0–5%

(b) 5–10%

(c) 10–20%

(d) 20–30%

FIGURE 8: The same as for Figure 4, but showing the results in the space $y_T - p_z$.

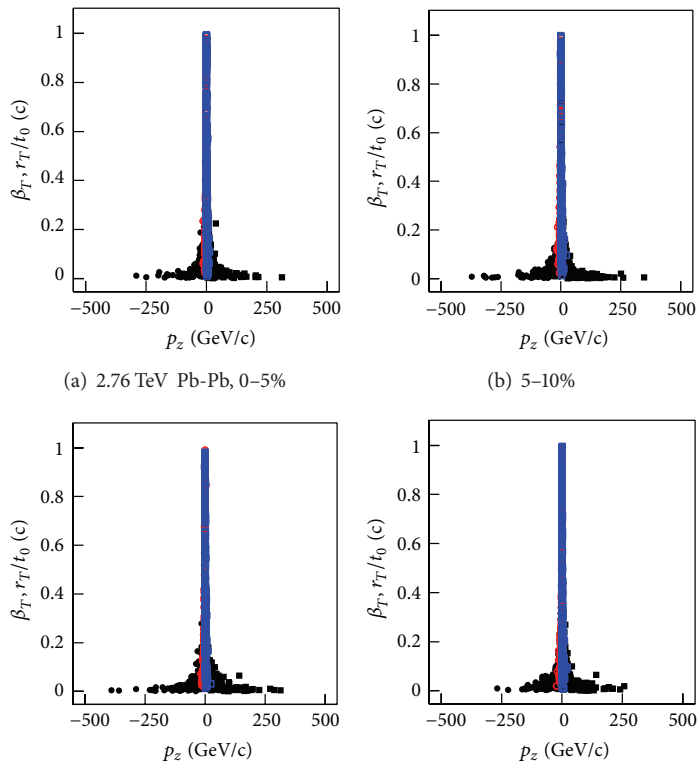

(a) 2.76 TeV Pb-Pb, 0–5% (b) 5–10%

(c) 10–20% (d) 20–30%

Figure 9: The same as for Figure 4, but showing the results in the space $\beta_T - p_z$ (or $r_T/t_0 - p_z$).

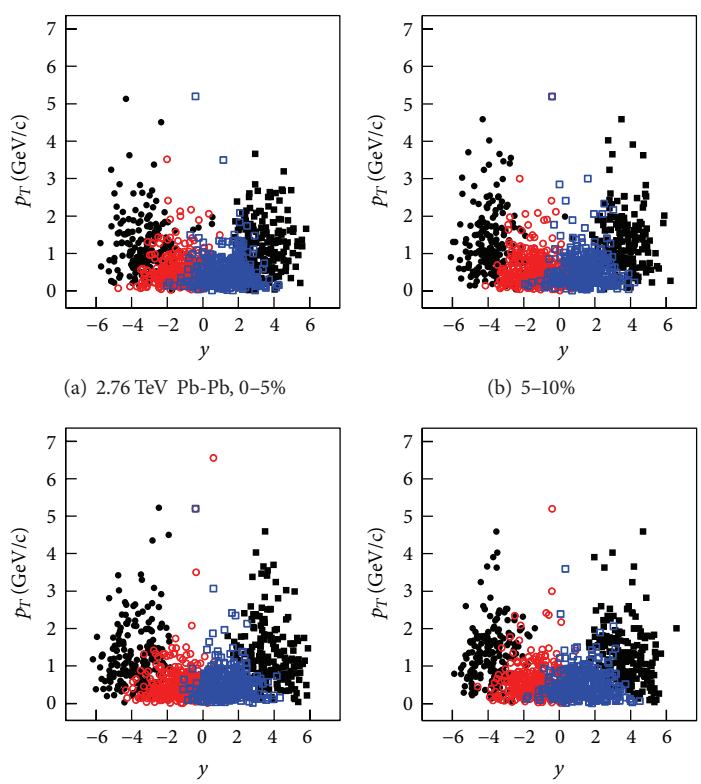

(a) 2.76 TeV Pb-Pb, 0–5% (b) 5–10%

(c) 10–20% (d) 20–30%

Figure 10: The same as for Figure 4, but showing the results in the space $p_T - y$.

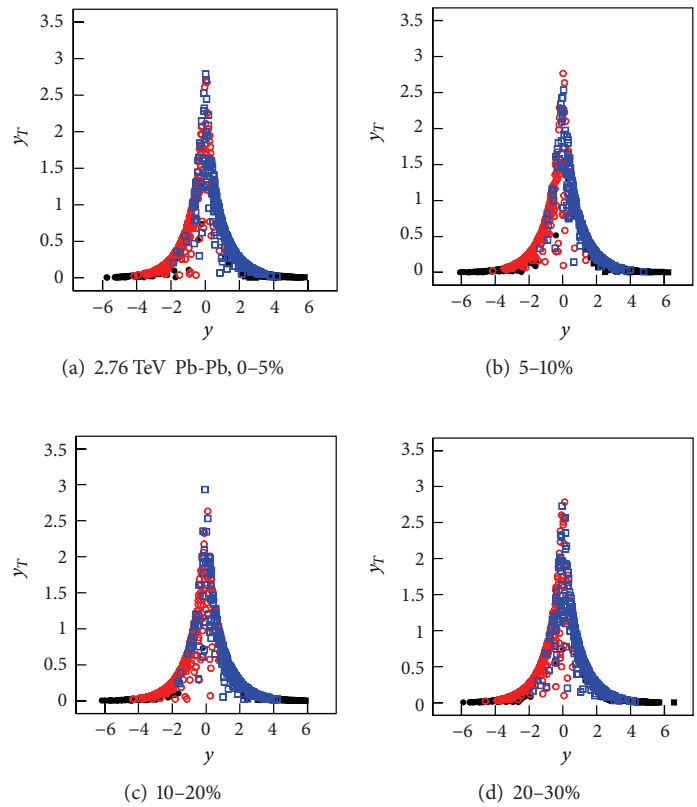

(a) 2.76 TeV Pb-Pb, 0–5%
(b) 5–10%
(c) 10–20%
(d) 20–30%

FIGURE 11: The same as for Figure 4, but showing the results in the space $y_T - y$.

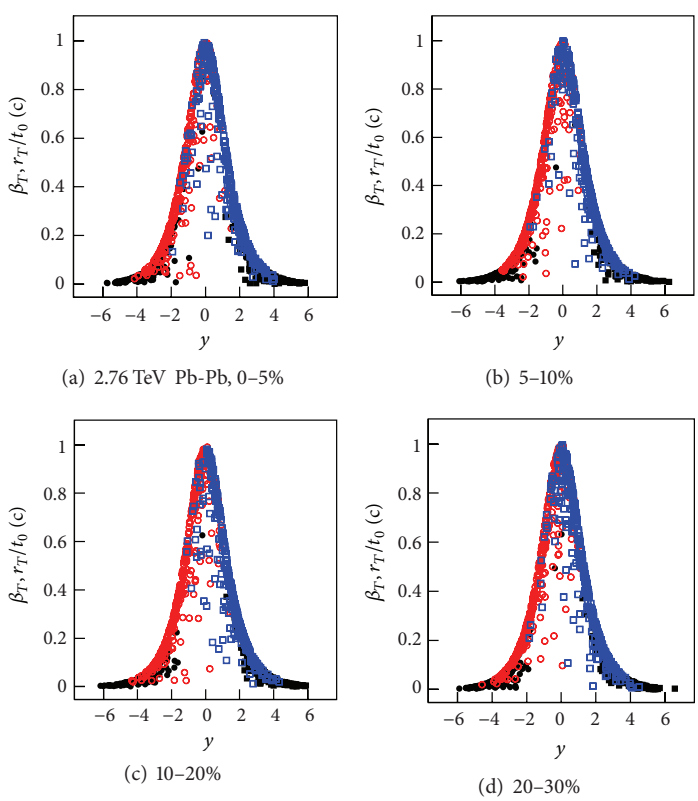

(a) 2.76 TeV Pb-Pb, 0–5%
(b) 5–10%
(c) 10–20%
(d) 20–30%

FIGURE 12: The same as for Figure 4, but showing the results in the space $\beta_T - y$ (or $r_T/t_0 - y$).

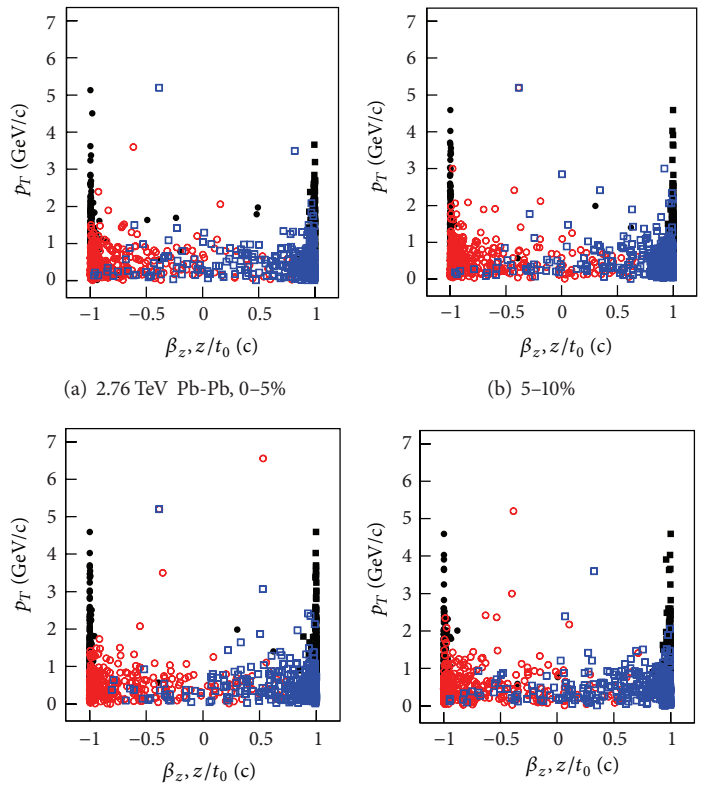

(a) 2.76 TeV Pb-Pb, 0–5%
(b) 5–10%
(c) 10–20%
(d) 20–30%

FIGURE 13: The same as for Figure 4, but showing the results in the space $p_T - \beta_z$ (or $p_T - z/t_0$).

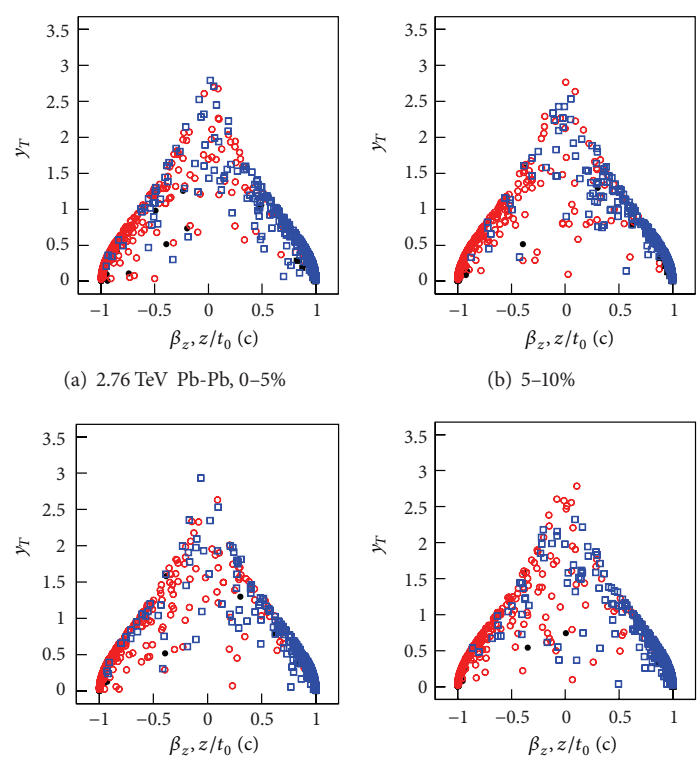

(a) 2.76 TeV Pb-Pb, 0–5%
(b) 5–10%
(c) 10–20%
(d) 20–30%

FIGURE 14: The same as for Figure 4, but showing the results in the space $y_T - \beta_z$ (or $y_T - z/t_0$).

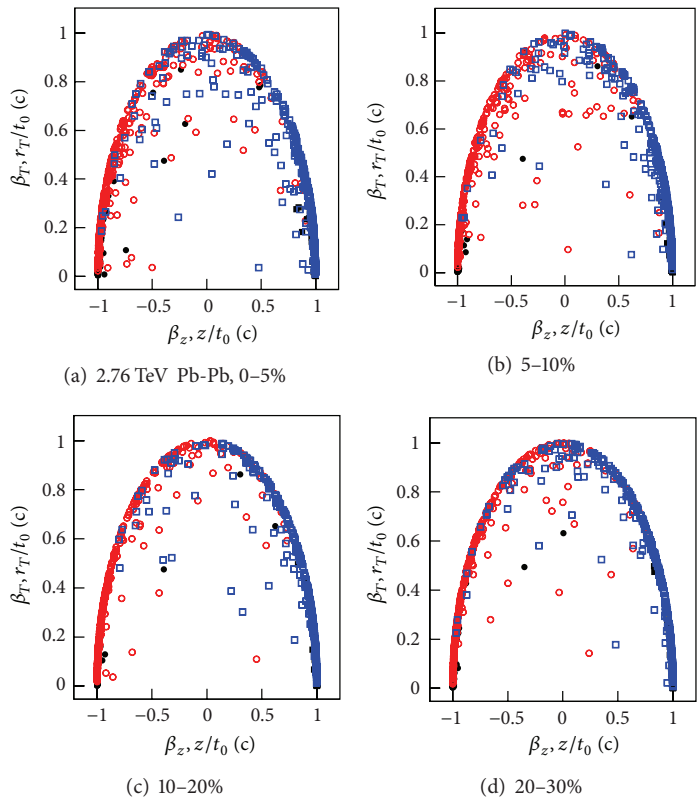

FIGURE 15: The same as for Figure 4, but showing the results in the space $\beta_T - \beta_z$ (or $\beta_T - z/t_0$ or $r_T/t_0 - \beta_z$ or $r_T/t_0 - z/t_0$).

obtained. The results for different centrality intervals are not obvious in the considered intervals from 0–5% to 20–30%.

Conflict of Interests

The authors declare that there is no conflict of interests regarding the publication of this paper.

Acknowledgments

This work was partly finished at the State University of New York at Stony Brook, USA. One of the authors (Fu-Hu Liu) thanks Professor Dr. Roy A. Lacey and the members of the Nuclear Chemistry Group of Stony Brook University for their hospitality. The authors acknowledge the supports of the National Natural Science Foundation of China (under Grant no. 10975095, no. 11247250, and no. 11005071), the China National Fundamental Fund of Personnel Training (under Grant no. J1103210), the Open Research Subject of the Chinese Academy of Sciences Large-Scale Scientific Facility (under Grant no. 2060205), and the Shanxi Scholarship Council of China, and the Overseas Training Project for Teachers at Shanxi University.

References

[1] I. G. Bearden, D. Beavisa, C. Besliu et al., "Charged particle densities from Au+Au collisions at $\sqrt{s_{NN}}$ = 130 GeV," *Physics Letters B*, vol. 523, no. 3-4, pp. 227–233, 2001.

[2] K. Adcox, S. S. Adler, and S. Afanasiev, "Formation of dense partonic matter in relativistic nucleus-nucleus collisions at RHIC: Experimental evaluation by the PHENIX collaboration," *Nuclear Physics A*, vol. 757, no. 1-2, pp. 184–283, 2005.

[3] B. B. Back, M. D. Baker, D. S. Barton et al., "Charged-particle pseudorapidity density distributions from Au+Au collisions at $\sqrt{s_{NN}}$ = 130 GeV," *Physical Review Letters*, vol. 87, no. 10, Article ID 102303, 4 pages, 2001.

[4] K. H. Ackermann, "Elliptic flow in Au+Au collisions at $\sqrt{s_{NN}}$ = 130 GeV," *Physical Review Letters*, vol. 86, no. 3, pp. 402–407, 2001.

[5] G. Aad, T. Abajyan, B. Abbott et al., "Search for new phenomena in events with three charged leptons at $\sqrt{s}$ = 7 TeV with the ATLAS detector," *Physical Review D*, vol. 87, no. 5, Article ID 052002, 33 pages, 2013.

[6] V. Khachatryan, A. M. Sirunyan, A. Tumasyan et al., "Upsilon production cross section in *pp* collisions at $\sqrt{s}$ = 7 TeV," *Physical Review D*, vol. 84, no. 11, Article ID 112004, 27 pages, 2004.

[7] R. Aaij, A. Beteta, A. Adametz et al., "Measurement of J/ψ production in *pp* collisions at $\sqrt{s}$ = 2.76 TeV," *The European Physical Journal C*, vol. 71, no. 5, Article ID 1645, 17 pages, 2011.

[8] B. Abelev, J. Adam, and D. Adamova, "Centrality dependence of π, K, and p production in Pb-Pb collisions at $\sqrt{s_{NN}}$ = 2.76 TeV,"

Physical Review C, vol. 88, no. 4, Article ID 044910, 23 pages, 2013.

[9] E. Abbas, B. Abelevbt, and J. Adam, "Centrality dependence of the pseudorapid ity density distribution for charged particles in Pb-Pb collisions at root $\sqrt{s_{NN}} = 2.76$ TeV," *Physics Letters B*, vol. 726, no. 4-5, pp. 610–622, 2013.

[10] S. Abreu, S. V. Akkelin, J. Alam et al., "Heavy ion collisions at the LHC—last call for predictions," *Journal of Physics G*, vol. 35, no. 5, Article ID 054001, 185 pages, 2008.

[11] F.-H. Liu, "Particle production in Au-Au collisions at RHIC energies," *Physics Letters B*, vol. 583, no. 1-2, pp. 68–72, 2004.

[12] F.-H. Liu, "Dependence of charged particle pseudorapidity distributions on centrality and energy in p(d)A collisions at high energies," *Physical Review C*, vol. 78, no. 1, Article ID 014902, 6 pages, 2008.

[13] F.-H. Liu, "Unified description of multiplicity distributions of final-state particles produced in collisions at high energies," *Nuclear Physics A*, vol. 810, no. 1–4, pp. 159–172, 2008.

[14] C. Tsallis, "Possible generalization of Boltzmann-Gibbs statistics," *Journal of Statistical Physics*, vol. 52, no. 1-2, pp. 479–487, 1988.

[15] C. Tsallis, "Nonadditive entropy and nonextensive statistical mechanics—an overview after 20 years," *Brazilian Journal of Physics*, vol. 39, no. 2, pp. 337–356, 2009.

[16] G. Wilk and Z. Włodarczyk, "Imprints of nonextensivity in multiparticle production," in *Proceedings of the 6th International Workshop on Relativistic Aspects of Nuclear Physics (RANP 2000)*, T. Kodama, C. E. Aguiar, H.-T. Elze, F. Grassi, Y. Hama, and G. Krein, Eds., pp. 78–96, October 2000, http://arxiv.org/abs/hep-ph/0011189v2.

[17] G. Wilk and Z. Włodarczyk, "Interpretation of the nonextensivity parameter q in some applications of Tsallis statistics and Levy distributions," *Physical Review Letters*, vol. 84, no. 13, pp. 2770–2773, 2000.

[18] G. Wilk and Z. Włodarczyk, "The imprints of nonextensive statistical mechanics in high-energy collisions," *Chaos, Solitons and Fractals*, vol. 13, no. 3, pp. 581–594, 2002.

[19] W. M. Alberico, P. Czerski, A. Lavagno, M. Nardi, and V. Soma', "Signals of non-extensive statistical mechanics in high-en ergy nuclear collisions," 2005, http://arxiv.org/abs/hep-ph/0510271v2.

[20] W. M. Alberico and A. Lavagno, "Non-extensive statistical effects in high-energy collisions," *The European Physical Journal A*, vol. 40, no. 3, pp. 313–323, 2009.

[21] G. Wilk and Z. Włodarczyk, "Multiplicity fluctuations due to the temperature fluctuations in high-energy nuclear collisions," *Physical Review C*, vol. 79, no. 5, Article ID 054903, 10 pages, 2009.

[22] J. L. Synge, *The Relativistic Gas*, North-Holland, Amsterdam, The Netherlands, 1957.

[23] C. D. Dermer, "The production spectrum of a relativistic Maxwell-Boltzmann gas," *The Astrophysical Journal*, vol. 280, no. 1, pp. 328–333, 1984.

[24] I. Sena and A. Deppman, "Systematic analysis of p_T-distributions in p + p collisions," *The European Physical Journal A*, vol. 49, no. 2, Article ID 17, 9 pages, 2013.

[25] J. Cleymans and D. Worku, "The Tsallis distribution in proton-proton collisions at $\sqrt{s} = 0.9$ TeV at the LHC," *Journal of Physics G*, vol. 39, no. 2, Article ID 025006, 12 pages, 2012.

[26] C. Wong and G. Wilk, "Tsallis fits to p_T spectra and multiple hard scattering in *pp* collisions at the LHC," *Physical Review D*, vol. 87, no. 11, Article ID 114007, 19 pages, 2013.